Chemical Science

RSC Publishing

EDGE ARTICLE

The role of statistics and microenvironment for the photoresponse in multi-switch architectures: The case of photoswitchable oligoazobenzene foldamers†‡

Cite this: *Chem. Sci.*, 2013, **4**, 4156

Zhilin Yu,[a] Steffen Weidner,[b] Thomas Risse*[c] and Stefan Hecht*[a]

Systems containing multiple photochromic units possibly display a synergistic interplay of individual switching events and hence potentially give rise to unprecedented photoresponsive behavior. Among such systems photoswitchable foldamers are attractive as the photoisomerization events are coupled to the helix–coil conformational transition. To gain comprehensive insight into the role of the number of switching units (statistics) as well as their specific location and relative orientation in the helix backbone, several series of foldamers have been synthesized and characterized. In these series of foldamers, the local environment of the photoswitchable units was precisely tuned as π,π-stacking interactions were enforced to occur between specific pairs, *i.e.* azobenzene–azobenzene, azobenzene–tolane, or phenylene–phenylene units. These particular arrangements are reflected not only in the stability of the helical conformation, but also affect the photoresponsive behavior, *i.e.* the rate of photoisomerization and extent of denaturation. Furthermore, determining the intramolecular spin–spin distance in a series of TEMPO-labeled foldamers with variable chain lengths and different spatial locations of the spin-labels deduced an independent verification of the photoinduced helix–coil transition by ESR spectroscopy. Quantitative analysis of the corresponding ESR spectra shows an excellent correlation of the extent of intramolecular spin–spin coupling and the intensity of the Cotton effect in CD spectroscopy. From all of these results an unusual relationship between the rate of photoisomerization and the extent of photoinduced denaturation could be unraveled, as they are not going hand-in-hand but compete with each other, *i.e.* the easier the individual switching event is, the harder it becomes to achieve a high degree of unfolding. This insight into the effect of microenvironment on the ease of individual switching events and the role of statistics on the resulting degree of the overall conformational transition is of general interest for the design of multi-switch architectures with improved photoresponse.

Received 14th June 2013
Accepted 29th July 2013

DOI: 10.1039/c3sc51664d

www.rsc.org/chemicalscience

Introduction

In organisms, most of fundamental physiological processes are sensitive to their local surrounding and require a specific microenvironment for their proper function.[1] Inspired by this phenomenon, the concept of realizing new functions by tuning the microenvironment has been very fruitful for the design of advanced, dynamic materials with unprecedented properties.[2] In principle, chemists create a suitable microenvironment around functional entities by either intramolecular modification using covalent functionalization schemes[3] or by altering the entire surrounding of the system using external additives, such as temperature, solvent, proton/ion concentration gradients, and photons.[4–7] In particular the latter, *i.e.* light, enables spatiotemporal regulation of a given function and the thereby derived active materials promise to be superior to their conventional static counterparts.

To address this challenge we have engaged in the design of photoswitchable functional molecular systems that can be controlled and even driven by light. The underlying design concept is based on harvesting the large structural changes caused by the light-induced *E–Z* isomerization of azobenzene photochromes.[8] For example, remote-controlled catalysts could be realized using light to regulate the accessibility of a reactive site.[9] A more complex case relates to the covalent connection of multiple photoresponsive units in order to amplify the incoming light stimulus into a geometrical/mechanical signal/output. For

[a]*Department of Chemistry, Humboldt-Universität zu Berlin, Brook-Taylor-Str. 2, 12489 Berlin, Germany. E-mail: sh@chemie.hu-berlin.de*

[b]*Bundesanstalt für Materialforschung und -prüfung (BAM), Richard-Willstätter-Strasse 11D, 12489 Berlin, Germany*

[c]*Institute of Chemistry and Biochemistry – Physical and Theoretical Chemistry, Freie Universität Berlin, Takustrasse 3, 14195 Berlin, Germany. E-mail: th.risse@fu-berlin.de*

† In memoriam Nicholas J. Turro.

‡ Electronic supplementary information (ESI) available: Synthetic details, compound characterization data, and description of the employed methods (56 pages). See DOI: 10.1039/c3sc51664d

this purpose, photoswitchable foldamers were designed,[10,11] in which the denaturation behavior was found to be dependent on the number as well as the location of the individual azobenzenes. While a large number of azobenzene units increases the likelihood of isomerization (statistics),[11c] their correct placement (microenvironment) allowed successive switching events to be coupled in a cooperative fashion.[12] Clearly, a particular microenvironment imparts a specific switching ability that presumably originates from a location-dependent energy barrier due to intrastrand π,π-stacking interactions, reflected in a higher content of *Z*-azobenzene at the helix termini.

Based on these considerations, it is crucial and also challenging to investigate how isomerization statistics in combination with azobenzene location affect the individual switching events and the denaturation of foldamer. As a result, the desire to vary the photochrome content while simultaneously positioning the individual azobenzene moieties precisely within the oligomeric backbone led us to generate several series of foldamers with different relative orientation of azobenzene moieties in the helices. Here, we report on the design and the synthesis of these series of foldamers and discuss their photoresponsive behavior with regard to the extent of isomerization and its impact on denaturation. In addition, functionalizing the backbone of the foldamer with spin-labels allowed us to investigate the conformational dynamics (helix–coil transition) using electronic spin resonance (ESR) and the results are compared to circular dichroism (CD) as a complementary technique that is typically used to monitor such conformational transitions.

Results and discussion

Molecular design and synthesis

Starting from the parent oligo(*meta*-phenylene ethynylene) (O*m*PE) foldamers,[13] connecting the azobenzene units by bridges of various lengths allows us to control the locations of azobenzene moieties within the backbone. For this purpose, either single ethynylene or kinked diethynylbenzene as well as diethynyltolane have been selected as connecting bridges of increasing length, which lead to three foldamer series composed of either 3 or 2 or 1.5 azobenzenes per turn (azos/turn). Furthermore, the length of the corresponding oligomers was chosen to insure that they adopt stable helically folded conformations in polar solvents. Therefore, seven foldamers, $\mathbf{10_5}$–$\mathbf{12_6}$–$\mathbf{14_7}$ and $\mathbf{11_4}$–$\mathbf{14_5}$ as well as $\mathbf{10_3}$–$\mathbf{14_4}$ (the first number denotes the number of phenylene units while the subscript indicates the number of azobenzene moieties) were designed and synthesized (Fig. 1).

With respect to the series of spin-labeled foldamers, two (2,2′,6,6′-tetramethylpiperidin-1-yl)oxyl (TEMPO)[14] moieties were covalently attached *via* amide linkages to the foldamer backbone with 2 azos/turn. To investigate the effect of chain length on the spin-coupling, two oligomers, *i.e.* undecamer $\mathbf{11_4}$-$\mathbf{TEMPO_{\alpha,\beta}}$ and heptadecamer $\mathbf{17_6}$-$\mathbf{TEMPO_{\alpha,\beta}}$, were designed (Fig. 2), while another comparison between $\mathbf{17_6}$-$\mathbf{TEMPO_{\alpha,\beta}}$ and $\mathbf{17_6}$-$\mathbf{TEMPO_{\alpha,\gamma}}$ allows us to determine the interaction of spin-labels with different spatial arrangements and hence distances at one and the same oligomer length. Low-temperature ESR spectra of dipolar coupled spin pairs can be analyzed to give the distance distribution between the two TEMPO units and further resulting in direct information about the corresponding conformation of the foldamer backbone (*vide infra*). In addition a meaningful analysis of the data for the doubly labeled molecules requires their comparison with a singly labeled variant – on the one hand to exclude possible intermolecular interactions and on the other hand to obtain an ESR spectrum of the spin label in its uncoupled state, necessary for distance determination. For this purpose a singly labeled oligomer $\mathbf{11_4}$-**TEMPO** was synthesized. In order to maintain the solubility in polar solvents and therefore benefit from the solvophobic driving force for folding, polar oligo(ethylene glycol) side chains have to be attached to each repeat unit of the foldamers *via* electron-deficient ester linkages.[15] Furthermore, chiral lactate-derived oligo(ethylene glycol) side chains were introduced and anticipated to induce a twist sense bias in the helical conformation thereby allowing us to investigate the chiral amplification and the conformation of backbones by CD spectroscopy.[16]

The different sequence-defined oligomers were obtained by efficient and mild Sonogashira–Hagihara coupling of appropriate acetylene- and halogen-terminated building blocks in an iterative divergent/convergent growth approach (Schemes S1–S2 and S4–S5, ESI‡). The proposed structures of all target oligomers were confirmed by proton nuclear magnetic resonance (^{1}H NMR) spectroscopy and matrix assisted laser desorption ionization – time of flight (MALDI-TOF) mass spectrometry as well as gel permeation chromatography (GPC). The characterization data for all investigated foldamers have been detailed thoroughly in the ESI.‡

Solvent-induced unfolding

The conformational preference of the oligomers in polar and nonpolar solvents was investigated mainly with the aid of optical spectroscopy. While UV/vis absorption spectroscopy is sensitive to changes between *transoid* and *cisoid* conformations reflected in the observed vibronic fine structure,[17] the occurrence of a bisignate Cotton effect in CD spectroscopy points to the presence of helical conformations and allows us to deduce the overall helix twist sense.[18,19] Treatment of the obtained denaturation data assuming a two-state model, *i.e.* a helix → coil transition from a poor to a good solvent (acetonitrile → chloroform), enables determination of the helix stabilization energies in the polar solvent.[15,17] The obtained $\Delta G(CH_3CN)$ values reflect the strength of π,π-stacking between aromatic units and therefore reveal the location and relative orientation of the azobenzenes moieties within the helical backbone.

Upon addition of chloroform to acetonitrile, the UV/vis absorption bands at 310 nm, generally assigned to the *transoid*-conformation,[17] increases for all foldamers (Fig. 3, top, S9 of ESI,‡ and ref. 11*c*), indicating the *cisoid* → *transoid* conformational transition and hence the unfolding of the all-*cisoid* helical conformation due to the disappearance of the solvophobic effect. Simultaneously, the intensities of the Cotton effect in the CD spectra for all tetradecameric foldamers (Fig. 3, bottom, S9 of ESI,‡ and ref. 11*c*) are comparable in acetonitrile and

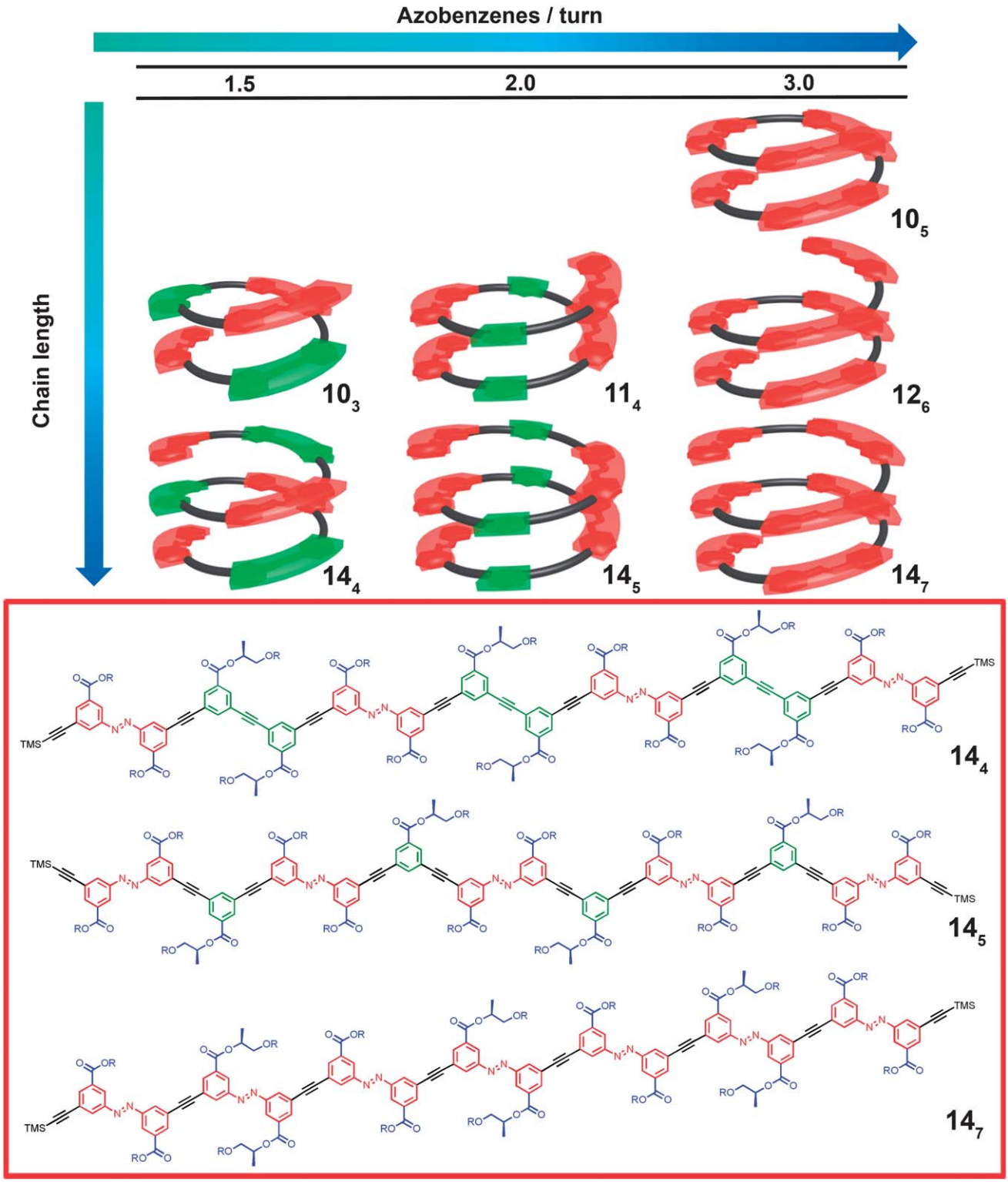

Fig. 1 Schematic representations of all oligomers by simplified folding cartoons (photoactive azobenzene moieties in red and photoinactive phenylene or tolane units in green) and chemical structures of the three tetradecameric oligomers $\mathbf{14_4}$, $\mathbf{14_5}$ and $\mathbf{14_7}$ (R = –$(CH_2CH_2O)_3CH_3$); in our nomenclature, the number 14 denotes the number of phenylene units, the subscript 4, 5 or 7 denotes the number of azobenzene units. For chemical structures of other foldamers, see Scheme S3, ESI.‡

decrease upon addition of chloroform until they completely vanish in neat chloroform. Interestingly, the different azobenzene : tolane chromophore ratios are reflected by the variable separation of their individual optical transitions in the CD spectra, as seen by the appearance of a shoulder at *ca.* 340 nm for $\mathbf{14_4}$, resembling a lower azobenzene content.

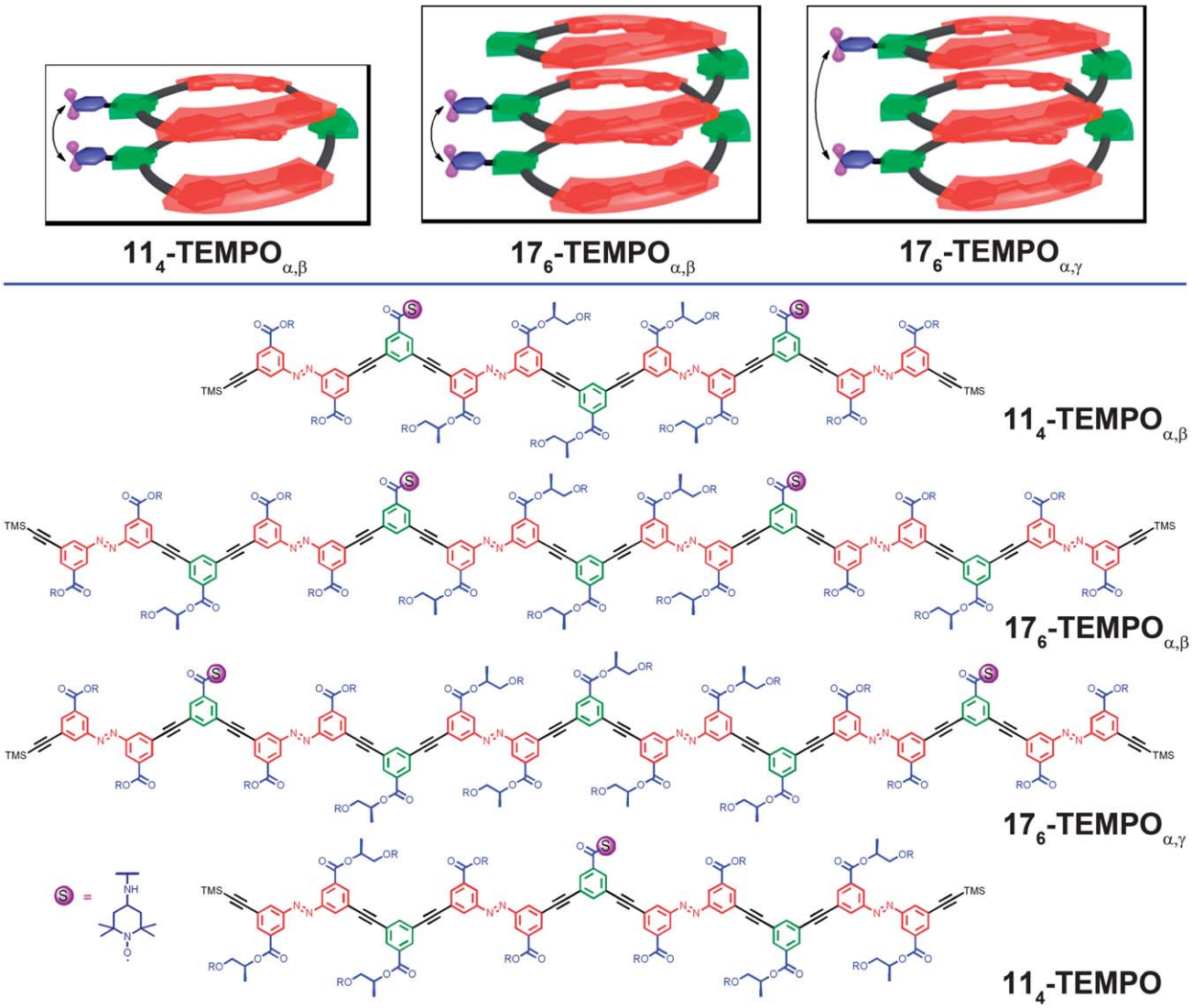

Fig. 2 Schematic representation of spin-labeled foldamers **11$_4$-TEMPO$_{\alpha,\beta}$**, **17$_6$-TEMPO$_{\alpha,\beta}$** and **17$_6$-TEMPO$_{\alpha,\gamma}$** (photoactive azobenzene moieties in red and photoinactive phenylene or tolane units in green, TEMPO spin labels in blue/purple) and their chemical structures as well as the one of reference compound **11$_4$-TEMPO** (R = –$(CH_2CH_2O)_3CH_3$, TEMPO connected to the backbone *via* amide bonds, *i.e.* –NH-TEMPO).

Effect of azobenzene location on helix stability

As indicated by molecular models, the relative orientations of azobenzenes within the helical structures either lead to π,π-stacking occurring solely between azobenzene units for the 3 and 2 azos/turn series (**10$_5$**–**12$_6$**–**14$_7$** and **11$_4$**–**14$_5$**) or enforce an alternating arrangement with π,π-stacking interaction[20] only between azobenzene and tolane units for the 1.5 azos/turn series (**10$_3$**–**14$_4$**). Therefore, three types of π,π-stacking interactions, *i.e.* azobenzene–azobenzene (azo–azo), phenylene–phenylene (Ph–Ph), and azobenzene–tolane (azo–tolane), contribute to the foldamers' stabilization energy (*vide supra*). Analysis of the solvent denaturation experiments qualitatively shows that, except the two shortest derivatives **10$_3$** and **10$_5$**, all oligomers fold into a stable helical structure in acetonitrile and quantitatively provides the corresponding helix stabilization energies $\Delta G(CH_3CN)$ (Table 1).[21] When again comparing the tetradecamers **14$_4$**, **14$_5$** and **14$_7$**, the foldamers having 2 or 3 azos/turn show a comparable helix stability while the 1.5 azos/turn helix appears to be somewhat less stable, *i.e.* helix stability follows the trend: **14$_7$** ≅ **14$_5$** > **14$_4$**. Importantly, from the measured $\Delta G(CH_3CN)$ values of foldamers **11$_4$**, **12$_6$**, **14$_4$**, **14$_5$** and **14$_7$**, the corresponding strengths of the three kinds of π,π-stacking interactions, *i.e.* azo–azo, Ph–Ph, and azo–tolane, can be estimated as −0.82, −0.44 and −0.71 kcal mol^{-1}, respectively (Fig. 4).

Based on the linear combination of the individual π,π-stacking interactions, a general formula for estimating the helix stabilization energy of azobenzene-containing O*m*PE foldamers in acetonitrile can be deduced from these values as:

$$\Delta G(CH_3CN)/\text{kcal mol}^{-1} = (-0.82)a + (-0.44)b + (-0.71)c \quad (1)$$

where *a*, *b*, and *c* stand for the number of the azo–azo, Ph–Ph and azo–tolane stacking interactions, respectively. Note that, the related $\Delta G(CH_3CN)$ values for foldamers obtained from this

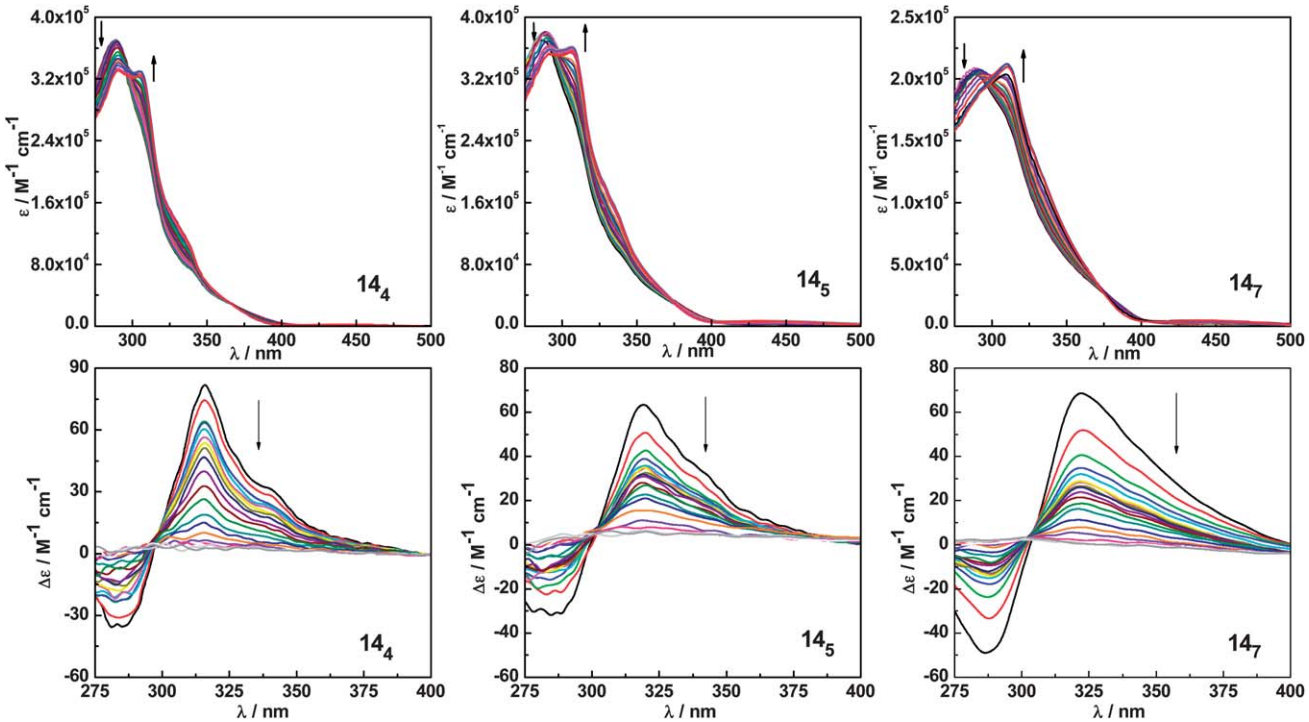

Fig. 3 UV/vis absorption (top) and CD (bottom) spectra of oligomers $\mathbf{14_4}$, $\mathbf{14_5}$ and $\mathbf{14_7}$ for solvent titration experiments ($CH_3CN \rightarrow CHCl_3$ with 5 vol% increments) at 25 °C.

equation are close to the corresponding values determined by the solvent titration experiment (Table 1). Therefore, it seems reasonable this equation allows us to calculate the stabilization energy $\Delta G(CH_3CN)$ of any related azobenzene foldamer that cannot be obtained from solvent titration experiments, such as $\mathbf{10_5}$ (-1.64 kcal mol^{-1}) and $\mathbf{10_3}$ (-1.42 kcal mol^{-1}) (Table 1). In addition – at least for the 3 azo/turn foldamer series, the enthalpy gained by addition of a single azobenzene repeat unit to the growing helix nucleus can be calculated according to the Zimm–Bragg two-state helix–coil thermodynamic model.[22] Thereby the initial entropic cost, *i.e.* the Gibbs free energy of helix nucleation $\Delta G_{nuc} = 1.15$ kcal mol^{-1} (involving three azobenzene units), is compensated by an enthalpic gain, *i.e.* the Gibbs free energy of helix propagation $\Delta G_{prop} = -1.15$ kcal mol^{-1} per added azobenzene unit, leading to a stable helical structure at chain lengths exceeding five azobenzene units.[23]

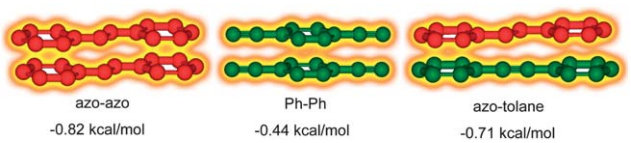

Fig. 4 The three types of π-stacking interaction contributing to helix stabilization in the different foldamer series and the corresponding strength derived from the stabilization energies of foldamers determined by the solvent titration experiment.

Photoinduced unfolding

The light-induced denaturation process, initiated by individual photoisomerization event(s) causing subsequent unfolding, was probed by both UV/vis absorption and CD spectroscopies for all investigated oligomers in the folding-promoting solvent

Table 1 The content of individual π-stacking interactions in all series of foldamers and their corresponding stabilization energy in CH_3CN at 25 °C

		1.5 azos/turn		2.0 azos/turn		3.0 azos/turn		
		$\mathbf{10_3}$	$\mathbf{14_4}$	$\mathbf{11_4}$	$\mathbf{14_5}$	$\mathbf{10_5}$	$\mathbf{12_6}$	$\mathbf{14_7}$
Number in helix	Azo–tolane	3	4	0	0	0	0	0
	Ph–Ph	0	0	1	2	0	0	0
	Azo–azo	0	0	2	3	2	3	4
$\Delta G(CH_3CN)$/kcal mol^{-1}	Exp.[a]	n.d.[c]	-2.83 ± 0.12	-2.04 ± 0.09	-3.38 ± 0.20	n.d.[c]	-2.30 ± 0.07	-3.45 ± 0.21
	Calc.[b]	-1.42	-2.84	-2.08	-3.34	-1.64	-2.46	-3.28

[a] Derived from UV/vis spectra. [b] Obtained from eqn (1). [c] Not determined due to incomplete folding in neat CH_3CN.

acetonitrile. Importantly, the evolution of the UV/vis absorption spectra reveals the signature of the photoisomerization reaction, *i.e.* vanishing π,π* and growing n,π* absorption bands, while the CD spectral changes indicate the transition from the helical to the random coil conformation.[11c] Previously we have shown that the intensity of the Cotton effect is a direct measure of the helix–coil conformational transition.[12] Therefore, the plots of UV/vis and CD absorption intensities as a function of time can be used to deduce the kinetic rate constants of the photoisomerization and the unfolding reactions, respectively.

Upon exposure of the foldamers to UV-light (358 nm), photoinduced azobenzene $E \rightarrow Z$ isomerization takes place as seen from the gradually decreasing π,π* absorption band at 289 nm as well as the weakly increasing n,π* transition at 450 nm, accompanied by an isosbestic point at *ca.* 405 nm in all foldamer series (Fig. 5, top, S12 of ESI‡ and ref. 11*c*). Simultaneously, the intensity of the Cotton effect in the CD spectra is continuously decreasing during the course of UV irradiation, indicating the depopulation of the (twist sense biased) helical conformation (Fig. 5, bottom, S12 of ESI,‡ and ref. 11*c*). The unfolding is most likely due to the vanishing π-stacking interactions involving non-planar *Z*-azobenzene moieties in the backbone. The remaining intensity of the Cotton effect in the photostationary state (PSS) was used to estimate the degree of unfolding (Table 2) assuming a two-state helix–coil model.

To investigate the distribution of the individual photoisomerization events within the backbone, the amount of *Z*-isomers formed until reaching the PSS was analyzed by ^{1}H NMR spectroscopy, which allows (partial) differentiation and quantification of the various azobenzene units (Table 2 and ESI‡). The *Z*-content of azobenzene ranges between 17.4% for the core unit of foldamer $\mathbf{14_7}$ all the way to 46.3% for the terminal units of foldamer $\mathbf{14_4}$, giving a comparable average amount of approximately 30% *Z*-isomers (Z_{av}) for all foldamers. In all foldamers the terminal azobenzene units have an apparently preferred tendency to isomerize, when compared to their internal or core counterparts. We attribute this preferred photoreactivity at the terminal units to a lower barrier of isomerization, which originates from breaking fewer π-stacking interactions, while isomerization of internal or core units would result in disruption of a larger number of π-contacts. In addition, photoisomerization at the single azobenzene core is disfavored for statistical reasons.

Comparing the rates of the individual processes for the different foldamer series (Table 2), there seems to be a general correlation between the rate of $E \rightarrow Z$ photoisomerization and denaturation: the higher the isomerization rates of the azobenzene units, the higher the rates of foldamer unfolding. The comparison of the tetradecamers reveals that an increasing azobenzene content leads to slower rates for both photoisomerization and unfolding, yet more complete denaturation (Fig. S16 of ESI‡). This apparent contradiction can be explained by the increasing barrier for isomerization due to stronger π-stacking interactions in the azobenzene-rich series, while at the same time an increasing number of azobenzene units statistically enhances the number of formed *Z*-isomers[24] (see last row in Table 2) and hence lead to increased levels of denaturation. Note that, considering the photoinduced denaturation, *i.e.* disrupting the related π-stacking interaction, it is reasonable to attribute the resulting level of the denaturation to the overall number of *Z*-isomers (*i.e.* the statistical chance), but not the average percentage. For instance, our prototype foldamer with one azobenzene core represents a greater average percentage of *Z*-isomers, and displays a less efficient denaturation. From this

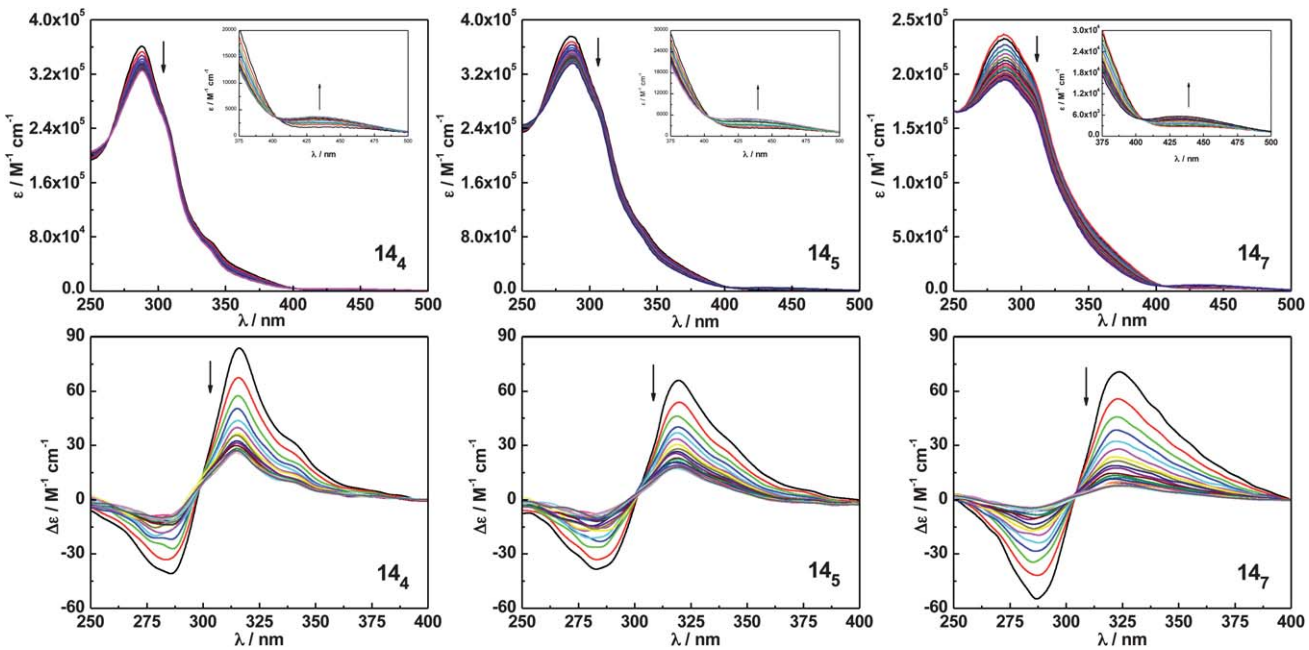

Fig. 5 UV/vis absorption (top) and CD (bottom) spectra of photochemical $E \rightarrow Z$ isomerization of oligomers $\mathbf{14_4}$, $\mathbf{14_5}$, and $\mathbf{14_7}$ during the course of irradiation at λ_{irr} = 358 nm in CH_3CN at 25 °C. The insets in the UV/vis absorption spectra show a magnification of the increasing n → π* absorption bands of the azobenzene units.

Table 2 Folding and photoswitching behavior of all investigated foldamers in CH_3CN at 25 °C

		1.5 azos/turn		2.0 azos/turn		3.0 azos/turn		
		10_3	**14_4**	**11_4**	**14_5**	**10_5**	**12_6**	**14_7**
$k(E \rightarrow Z)^a/[\times 10^2\ s^{-1}]$		2.84 ± 0.05	1.22 ± 0.01	1.85 ± 0.05	0.83 ± 0.02	2.62 ± 0.05	1.53 ± 0.08	0.84 ± 0.02
$k(\text{unfolding})^b/[\times 10^2\ s^{-1}]$		4.44 ± 0.05	1.38 ± 0.03	2.72 ± 0.07	1.21 ± 0.02	5.17 ± 0.11	2.88 ± 0.03	1.13 ± 0.03
Photoinduced [unfolded]^b (%)		93	67	83	73	92	90	87
Z-Content in PSS^c (%)	$Z_{term}{}^c$	n.d.^{d}	46.3 ± 0.3	43.4 ± 0.4	45.5 ± 0.5	n.d.^{d}	43.3 ± 0.3	39.8 ± 0.2
	$Z_{int\text{-}1}{}^c$	n.d.^{d}	20.5 ± 0.5	28.4 ± 0.4	31.3 ± 0.3^g	n.d.^{d}	27.5 ± 0.5	24.9 ± 0.1^g
	$Z_{int\text{-}2}{}^c$	n.d.^{d}	—^{e}	—^{e}	—^{e}	n.d.^{d}	—^{e}	17.4 ± 0.4
	$Z_{core}{}^c$	n.d.^{d}	—^{f}	—^{f}	31.3 ± 0.3^g	n.d.^{d}	29.5 ± 0.5	24.9 ± 0.1^g
	$Z_{av}{}^c$	n.d.^{d}	33.4 ± 0.6	35.9 ± 0.6	36.9 ± 0.6	n.d.^{d}	33.4 ± 0.6	27.1 ± 0.1
Number of *Z*-azobenzene	n.d.^{d}	1.3	1.4	1.8	n.d.^{d}	2.0	1.9	

^{a} Derived from UV/vis spectra. ^{b} Derived from CD spectra. ^{c} Determined by ^{1}H NMR spectroscopy (Z_{term}, $Z_{int\text{-}1}$, $Z_{int\text{-}2}$ and Z_{core} refer to the percentage of *Z*-azobenzene as compared to individual all-*E* units in the terminal, the first/second internal, or core positions, respectively, Z_{av} = mathematical average). ^{d} Not determined due to incomplete folding in neat CH_3CN. ^{e} There is only one internal azobenzene in foldamers **14_4**, **11_4**, **14_5** and **12_6**. ^{f} There is no core azobenzene in foldamers **14_4** and **11_4**. ^{g} One kind of internal azobenzene unit (int-1) cannot be distinguished from the core azobenzene unit, and hence their (identical) average value is given.

finding two opposing design parameters can be deduced. On the one hand, enhancing the number of azobenzene units is favorable as it increases the statistical chances for light-induced formation of helix-breaking *Z*-isomers. On the other hand, avoiding strong π-stacking interactions, in particular between cofacial azobenzene units (as in the 1.5 azo/turn series, *i.e.* **14_4**), enhances the efficiency of the photoisomerization and unfolding. Therefore, both chain length and azobenzene distribution throughout the backbone has to be optimized to realize highly efficient photoswitchable foldamer systems.

Refolding induced by thermal $Z \rightarrow E$ isomerization

While the denaturation triggered by photoinduced $E \rightarrow Z$ isomerization necessitates ultrafast time-resolved spectroscopy to deduce the dynamics of the entire process,[25] the thermally induced renaturation due to $Z \rightarrow E$ isomerization should be determined more easily owing to the convenient time frames of *Z*-azobenzene with general half-lives of the order of hours. To straightforwardly investigate the conformational coil → helix transition, the thermally induced refolding of oligomers was characterized by CD spectroscopy in aqueous acetonitrile solution.[26]

When keeping the irradiated oligomer samples in the dark, the thermal $Z \rightarrow E$ isomerization of azobenzene occurs gradually as evident from the increase of the Cotton effect belonging to the reformed helices (Fig. S17–19 of ESI‡). The recovery of the CD signal as a function of time reveals that the thermally induced refolding of the oligomers proceeds by anticipated first-order kinetics (Table 3 and Fig. S24–26 of ESI‡).[27] The refolding rate constants of the three tetradecamers show an obvious decrease upon heating and the oligomers containing fewer azobenzene units exhibit a faster renaturation to their helical conformation. Based on a van't Hoff type analysis, the activation parameters of thermally induced refolding of oligomers can be obtained (Fig. S27 of ESI‡).[28] In contrast to previous reports of simple azobenzene derivatives,[9b,29] the investigated azobenzene oligomers display enthalpies and entropies of activation for their refolding processes, *i.e.* $\Delta H_f^{\ddagger}$ and $\Delta S_f^{\ddagger}$, which are both negative. The resulting activation energies $\Delta G_f^{\ddagger}$ are mainly attributed to the entropic component, *i.e.* $\Delta S_f^{\ddagger}$. This clearly shows that refolding of the oligomers is associated with an increase of structural order, for which an entropic penalty has to be paid.

However, the kinetic rate constants and the underlaying $\Delta G_f^{\ddagger}$ values for the refolding processes in these multi-azobenzene systems are comparable to the corresponding values for thermal $Z \rightarrow E$ isomerization in single azobenzenes, indicating that there is no simple addition of individual isomerization events. By plotting the thermodynamic parameters of tetradecamers as well as of parent azobenzene, an evident compensation relationship with good linearity ($R = 0.999$) between them was found (Fig. S28 of ESI‡). Importantly, this result implies that despite of being incorporated into rigid structures, the azobenzene moieties within all backbones isomerize *via* an identical mechanism.[30]

Meanwhile, the evolution of the CD signals of oligomer **12_6**, which could quantitatively be photodenaturated, was observed as an evident sigmoidal shape distribution during the refolding process (Fig. 6, top). In contrast, such a distribution is not appearing in the cases of tetradecameric oligomers, perhaps due to the existence of residual helices arising from the non-negligible all-*E* isomer in PSS (Fig. 6, top). This assumption was supported by the experiments of relaxing the samples **14_4**, **14_5** and **14_7** in aqueous acetonitrile solution from the PSS obtained in chloroform,[31] in which the *Z*-content of azobenzenes is higher than in acetonitrile and resulting a smaller residual helix content. As a result, the refolding of tetradecamers shows a region with slow increase of CD intensity at the beginning similar to the oligomer **12_6** and leading to a sigmoidal distribution of the CD signals (Fig. 6, bottom). In analogy to the known cooperative (un)folding in the solvent-induced process,[16] it is reasonable to assume that the refolding of oligomers during thermal *Z*–*E* isomerization is also a cooperative process.[32]

Table 3 Activation parameters of refolding for tetradecamers induced by thermal $Z \rightarrow E$ isomerization as determined by CD spectroscopy

	Rate constant/[$\times 10^5$ s^{-1}]					
	15 °C	25 °C	35 °C	$\Delta H_f^{\ddagger}$/kcal mol^{-1}	$\Delta S_f^{\ddagger}$/cal mol^{-1} k^{-1}	$\Delta G_f^{\ddagger}$ (25 °C)/kcal mol^{-1}
$\mathbf{14_4}$	8.32 ± 0.06	7.24 ± 0.05	6.24 ± 0.06	−3.12 ± 0.10	−87.9 ± 0.35	23.1
$\mathbf{14_5}$	6.01 ± 0.88	5.59 ± 0.28	5.15 ± 0.11	−1.95 ± 0.08	−84.5 ± 0.27	23.2
$\mathbf{14_7}$	3.02 ± 0.10	2.43 ± 0.09	2.08 ± 0.09	−3.89 ± 0.24	−92.7 ± 0.81	23.7

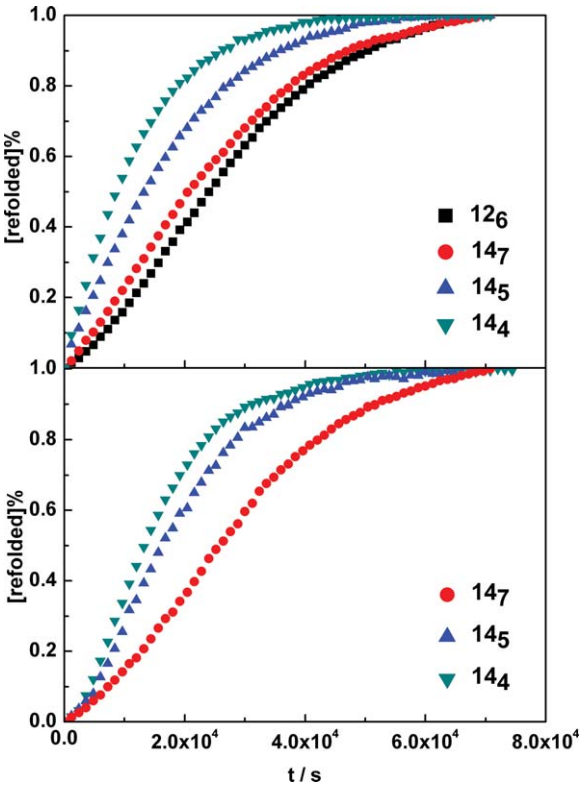

Fig. 6 The changes of CD signals as functions of time during azobenzene thermal $Z \rightarrow E$ isomerization in oligomers $\mathbf{12_6}$, $\mathbf{14_4}$, $\mathbf{14_5}$ and $\mathbf{14_7}$ in aqueous CH_3CN solution (v/v, 4/1) from PSS in CH_3CN (top) or $CHCl_3$ (bottom) at 25 °C.

ESR spectroscopy investigation

Although a number of computational methodologies have been utilized to simulate the conformational transition of peptides and foldamers,[33] only few experimental investigations addressing the transition of aromatic foldamers have been reported thus far.[34] At the microscale level, ESR spectroscopy has been extensively applied to characterize molecular conformations *via* checking the information of the precise distance or distance distributions ranging from 1 to around 5–6 nm, which can be derived from dipolar interaction between two spin centers.[35] In contrast to CD spectroscopy, the determination of the distance distribution by ESR spectroscopy does not rely on a particular helical screw sensor, rendering this as a complementary technique for the confirmation of backbone conformations.[36] Assuming a relatively rigid conformation of the TEMPO units, it is expected that all-*E* azobenzene resulting in helical structures, will be associated with a rather small intramolecular distance of the spin labels as compared to the photoinduced coil structure, where the lack of secondary structure should lead to an increase of the inter-spin distance. Based on this consideration, ESR spectroscopy can be used to verify the conformational transition as well as further follow the kinetics of refolding.

Prior to the ESR experiments, the stability of the spin-labeled foldamers in polar solvent and their photoinduced unfolding processes were determined by UV/vis absorption and CD spectroscopies. Based on solvent titration experiments, the $\Delta G(CH_3CN)$ values are obtained as −2.41 and −3.79 kcal mol^{-1} for $\mathbf{11_4}$-$\mathbf{TEMPO_{\alpha,\beta}}$ and $\mathbf{17_6}$-$\mathbf{TEMPO_{\alpha,\beta}}$, respectively (Fig. S31, ESI‡). In addition, the residual intensities of the Cotton effect in CD spectra in PSS for the spin-labeled foldamers were manifested as 86% and 56% for $\mathbf{11_4}$-$\mathbf{TEMPO_{\alpha,\beta}}$ and $\mathbf{17_6}$-$\mathbf{TEMPO_{\alpha,\beta}}$, respectively (Fig. S33, ESI‡). Interestingly, the resulting values for $\mathbf{11_4}$-$\mathbf{TEMPO_{\alpha,\beta}}$ are comparable to those of the cousin foldamer $\mathbf{11_4}$, demonstrating that the stability and the photoinduced denaturation of foldamer are only slightly affected by the replacement of the glycol side chain by the spin-label.

The continuous-wavelength ESR (cw-ESR) spectra of the spin-labeled foldamer series were measured in acetonitrile at 20 K to ensure that residual motion of the molecules does not influence the dipolar coupling of the spin labels (Fig. 7). The concentration of the solutions were chosen such that the intermolecular spin–spin interactions can be ignored as probed by the singly labeled foldamer $\mathbf{11_4}$-$\mathbf{TEMPO}$. Upon UV light irradiation, the ESR spectra of all spin-labeled foldamers show a reduction of the line width most clearly seen by the formation of a more pronounced valley between the two low field maxima. This reduction of the line width is directly related to a weakened dipolar spin–spin interaction, which is particularly apparent for the foldamer $\mathbf{17_6}$-$\mathbf{TEMPO_{\alpha,\gamma}}$. The observed decrease of the dipolar coupling clearly proves the increased distance between the spin probes upon light irradiation, hence the loss of a compact backbone conformation.

A quantitative analysis of the coupled spectra by means of a Fourier-deconvolution with the spectrum of non-interacting spin labels (singly labeled $\mathbf{11_4}$-$\mathbf{TEMPO}$) allows us to determine the intramolecular distance distribution between the spin labels.[37] Fig. 8 shows the result of such an analysis for $\mathbf{17_6}$-$\mathbf{TEMPO_{\alpha,\gamma}}$ prior and after light irradiation using either a simple box-like distribution of distances optimized by a least-square fit procedure (black trace) or a distribution as determined by a Tikhonov regularization of the data (red trace).[38] The first thing to note is that the molecules do not exhibit a

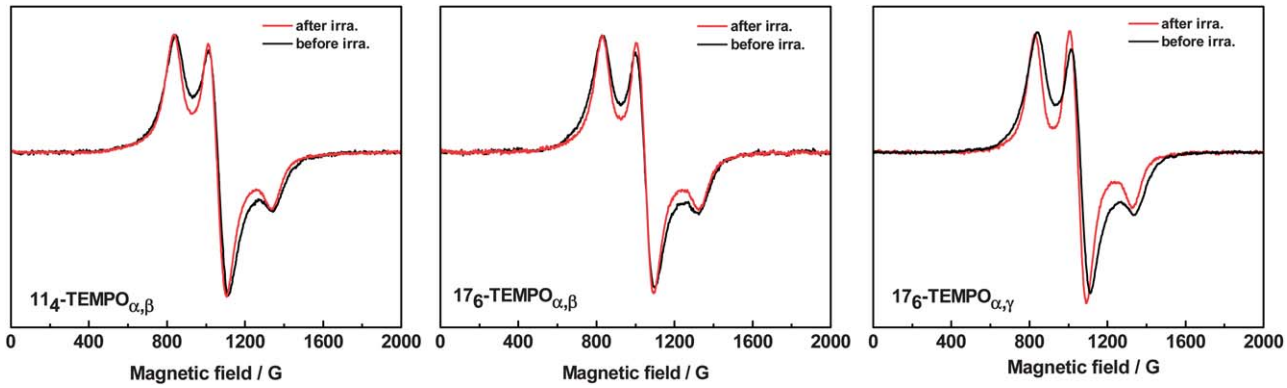

Fig. 7 The cw-ESR spectra of spin-labeled foldamers **11_4-TEMPO$_{\alpha,\beta}$**, **17_6-TEMPO$_{\alpha,\beta}$** and **17_6-TEMPO$_{\alpha,\gamma}$** before (dark) and after (red) UV irradiation (358 nm) recorded in acetonitrile at 20 K.

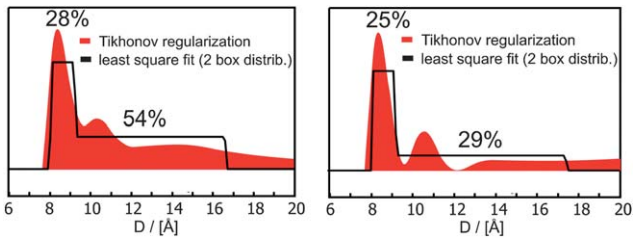

Fig. 8 The distance distribution extracted from cw-ESR spectra of foldamer **17_6-TEMPO$_{\alpha,\gamma}$** before (left) and after (right) UV light irradiation in acetonitrile at 20 K. In addition, a fraction of molecules show a conformation with a distance of spin labels larger than 2 nm not detected as broadening in the cw-ESR experiment. This fraction is 18% (left) and 46% (right), respectively.

single well defined interspin distance even for the folded molecule prior to exposure to light. In fact the molecule shows a rather broad distance distribution ranging from about 0.9 nm all the way to 2 nm, which is the upper distance limit of the cw-ESR experiment used here.[38] The distance distribution can be understood by the conformational flexibility of the TEMPO side chain. Upon light irradiation, there is an evident change in the distance distribution of **17_6-TEMPO$_{\alpha,\gamma}$**. The weight of distances larger than 2 nm increase by a factor of about 2 at the main expense of distances in the range between 1 and 2 nm. The distance component at 0.9 nm is reduced by about 15% only. With the given signal to noise ratio of the spectra, which is set by the low concentration required to avoid intermolecular interactions, the uncertainty in determining this small distance, *i.e.* lower than 1 nm contribution is rather large.[39] The observed changes in the distance distribution between 1 and 2 nm are in very good agreement with expectations based on CD spectroscopy, which showed a residual Cotton effect of 56%, implying that less than half of the molecules are unfolded. In turn this implies that approximately 50% of the molecules in the PSS are in their folded conformation in agreement with the observed reduction of the dipolar coupled contribution of the spectrum by 50%. This in fact can be interpreted such that the molecules in the unfolded state have an intramolecular spin–spin distance larger than 2 nm, which is beyond the sensitivity of the cw-experiments. Qualitatively the same trend can be deduced for the other two foldamers shown in Fig. 7, however, the effect on the spectrum is much smaller due to the smaller content of unfolded molecules in the PSS, which in turn renders a quantitative comparison difficult.

In addition, cw-ESR spectroscopy was utilized to detect the kinetics of the thermally induced refolding as an alternative method to CD spectroscopy as discussed above. Again the spectrum of **17_6-TEMPO$_{\alpha,\gamma}$** was used to investigate the temporal evolution of the spectra. The challenge for this investigation arises from the fact that the spectrum for the unfolded state is not known. To circumvent this complication the temporal evolution of the spectra is described by the amplitude ratio (d_1/d_0) (Fig. 9, center), which can serve a qualitative measure for dipolar coupling of spin labels.[40] The analysis of the ESR spectra shown in the left panel of Fig. 9 reveals the d_1/d_0 ratio to increase over time and return to the value prior to the light excitation. Thus, the change of the amplitude ratio can be identified with readoption of the helical conformation associated with a smaller average distance between the spin labels. Interestingly, the d_1/d_0 ratio shows a sigmoidal type of behavior with a half-life time of the random coil structure of 44 h. However, the corresponding change of the Cotton effect for the foldamer **17_6-TEMPO$_{\alpha,\gamma}$** in acetonitrile during azobenzene thermal isomerization shows an exponential evolution, which was similar to the results of tetradecameric foldamers (Fig. 9, right). The difference between the two experiments may be explained by the grossly different physics determining the respective signals. The intensity of the Cotton effect may depend rather strongly on individual isomerization events within the molecules and is associated with the difference of molar circular dichroism between various intermediate folding 'cousins', while the broadening of the ESR spectra is solely dependent on the interspin distance, with the additional boundary condition that only distances below 2 nm lead to an observable broadening, which may render ESR spectroscopy insensitive to individual isomerization events. Nevertheless, the shape of the amplitude ratio over time suggests that the corresponding process is cooperative, in accordance with the effects discussed above.

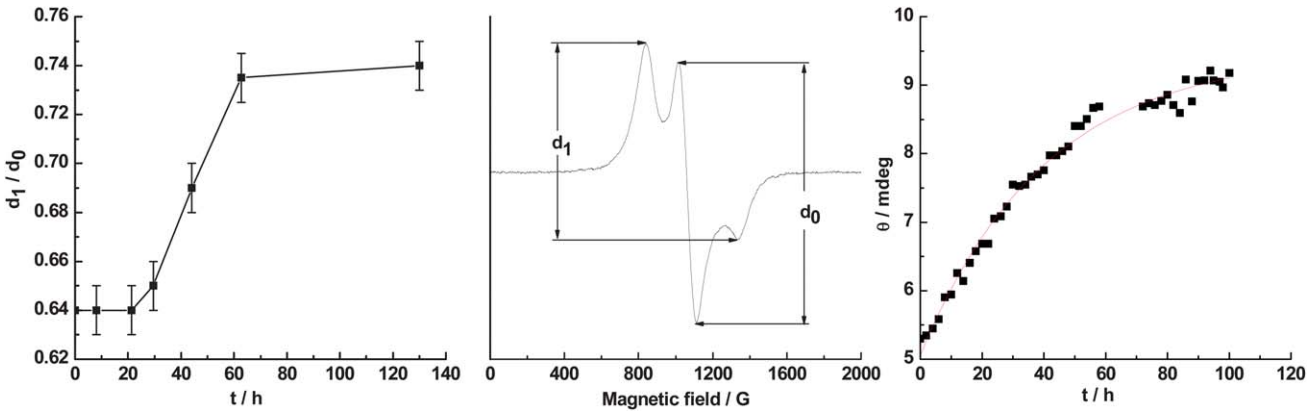

Fig. 9 Time dependence of the amplitude ratio of d_1/d_0 of the ESR spectra (left) and the intensity of Cotton effect in CD spectra (right) for the foldamer **17_6-TEMPO$_{\alpha,\gamma}$** during the thermal isomerization of azobenzene at room temperature. The definition of the amplitude ratio of d_1/d_0 (the d_1/d_0 ratios at initial and PSS states are 0.74 and 0.64, respectively) is given in the center panel.

Conclusion

In summary, three foldamer series with backbones composed of photo-static aromatic and photo-active azobenzene moieties were prepared by multi-step synthesis involving Sonogashira–Hagihara coupling as the key method. Within these foldamer series, the stability of the folded conformation in the folding-promoting solvent acetonitrile was governed by the number and relative orientation of azobenzene moieties in the helices, in accordance with discrete π,π-stacking interactions between aromatic units, *i.e.* azobenzene–azobenzene, azobenzene–tolane and phenylene–phenylene. Based on the stabilization free energies determined by the solvent titration experiments, the strength of the individual π,π-stacking interactions could be derived and should prove useful for predicting the stability of foldamers with related sequence. With regard to the foldamers' photoresponsive behavior we find that increasing the number of azobenzene units in the backbone naturally leads to an enhanced *Z*-azobenzene content (purely based on statistics) and in turn facilitates foldamer denaturation. On the contrary, the efficiency of photoisomerization and denaturation is enhanced in foldamers with lower azobenzene content and specific orientations, which allow strongly π-stacked azobenzene–azobenzene interactions to be avoided. This investigation demonstrates that the combination of the microenvironment and the relative orientation of the azobenzene moieties in the helices gives rise to a competing relationship between the rate and the extent of photoinduced denaturation. In agreement with our previous results,[11c] both chain length and azobenzene distribution throughout the helical backbone play a key role in the photoinduced behavior of the foldamers. Furthermore, the study of the azobenzene thermal isomerization can be used to determine the activation parameters for refolding, which indicate that the refolding process is mainly driven by the entropic loss due to confining the foldamers in an ordered helical conformation. From the observed enthalpy–entropy compensation a uniform isomerization pathway for the individual azobenzene moieties can be deduced. In addition, the photoinduced conformational transition of foldamers was characterized by ESR spectroscopy in a series of TEMPO-functionalized foldamers exploiting the distance-dependence of intramolecular spin–spin coupling. This approach directly and independently from CD confirms that the photoisomerization of azobenzene gives rise to the untwisting of the compact helical backbone. Importantly, the refolding kinetics of the irradiated foldamer can be investigated by recording the intramolecular distances of spin-labels over time, showing a cooperative refolding process more clearly than the CD method.

In this study, the location-dependent switching ability of azobenzene moieties within photoswitchable foldamers and more generally well-defined molecular frameworks has been demonstrated, which should prove useful for the design of highly light-responsive molecular systems. To further advance our studies in such multi-photochrome architectures, we are currently investigating the role of energy transfer between switching units within the foldamer backbone. By implementing different switching units and therefore introducing internal energy gradients we are aiming at funneling the excitation energy to specific photoactive sites in the helix in order to further enhance the photoresponse of the system. To gain detailed insight into the underlying mechanism, it will be crucial to involve novel approaches to characterize the photoinduced conformational transition, ideally combining both experimental as well as theoretical methods to study dynamics.[33,41] The remarkable geometrical extension-shrinkage of photoswitchable foldamers, resulting from the conformational transition, offers the possibility to remote-control a variety of functional molecular systems and processes. Along this line, our efforts are being devoted to utilize such photoswitchable foldamers in sophisticated light-controlled catalysts[2c] as well as molecular walkers[42] for optomechanical systems.[43]

Acknowledgements

The authors thank Jutta Schwarz for synthesizing large quantities of enantiomerically pure oligo(ethylene glycol) side chain. Generous support by the German Research Foundation (DFG *via* SFB 765) and the European Research Council (*via*

ERC-2012-STG_308117 "Light4Function") is gratefully acknowledged. BASF AG, Bayer Industry Services, and Sasol Germany are thanked for generous donations of chemicals.

Notes and references

1 For microenvironment regulated biological processes, see: (*a*) P. R. O. de Montellano, *Cytochrome P-450: Structure, Mechanism and Biochemistry*, Plenum, New York, 1995; (*b*) H. J. Kong and D. J. Mooney, *Nat. Rev. Drug Discovery*, 2007, **6**, 455–463; (*c*) J. A. Joyce and J. W. Pollard, *Nat. Rev. Cancer*, 2008, **9**, 239–252; (*d*) J. P. Medema and L. Vermeulen, *Nature*, 2011, **474**, 318–326.

2 For artificial functional materials including local environment-control, see: (*a*) A. W. Bosman, H. M. Janssen and E. W. Meijer, *Chem. Rev.*, 1999, **99**, 1665–1688; (*b*) S. Hecht and J. M. J. Fréchet, *Angew. Chem., Int. Ed.*, 2001, **40**, 74–91; (*c*) R. S. Stoll and S. Hecht, *Angew. Chem., Int. Ed.*, 2010, **49**, 5054–5075.

3 For related examples of local environment affected functional activity: (*a*) K. J. Shea and D. Y. Sasaki, *J. Am. Chem. Soc.*, 1989, **111**, 3442–3444; (*b*) C. J. Hawker, K. L. Wooley and J. M. J. Fréchet, *J. Am. Chem. Soc.*, 1993, **115**, 4375–4376; (*c*) F. Würthner and J. Rebek, *J. Chem. Soc., Perkin Trans. 2*, 1995, 1727–1734; (*d*) R. Cacciapaglia, S. Di Stefano and L. Mandolini, *J. Am. Chem. Soc.*, 2003, **125**, 2224–2227; (*e*) D. Sud, T. B. Norsten and N. R. Branda, *Angew. Chem., Int. Ed.*, 2005, **44**, 2019–2021; (*f*) Y. Vakrat-Haglili, L. Weiner, V. Brumfeld, A. Brandis, Y. Salomon, B. Mcllroy, B. C. Wilson, A. Pawlak, M. Rozanowska, T. Sarna and A. Scherz, *J. Am. Chem. Soc.*, 2005, **127**, 6487–6497.

4 For solvent-induced cooperative folding properties, see: (*a*) D. J. Hill, M. J. Mio, R. B. Prince, T. S. Hughes and J. S. Moore, *Chem. Rev.*, 2001, **101**, 3893–4012; (*b*) S. Hecht and I. Huc, *Foldamers: Structure, Properties, and Applications*, Wiley-VCH, Weinheim, 2007.

5 For ion or pH-stimulus molecular machines, see: (*a*) V. Balzani, F. Credi, M. Raymo and J. F. Stoddart, *Angew. Chem., Int. Ed.*, 2000, **39**, 3348–3391; (*b*) J. F. Stoddart, Special Issue on Molecular Machines, *Acc. Chem. Res.*, 2001, **34**, 410–522.

6 For temperature or pH-stimulus drug release, see: (*a*) R. Klajn, J. F. Stoddart and B. A. Grzybowski, *Chem. Soc. Rev.*, 2010, **39**, 2203–2237; (*b*) M. A. C. Stuart, W. T. S. Huck, J. Genzer, M. Müller, C. Ober, M. Stamm, G. B. Sukhorukov, I. Szleifer, V. V. Tsukruk, M. Urban, F. Winnik, S. Zauscher, I. Luzinov and S. Minko, *Nat. Mater.*, 2010, **9**, 101–113.

7 For comprehensive research of photochromism: (*a*) B. L. Feringa, *Molecular Switches*, Wiley-VCH, Weinheim, 2nd edn, 2011; (*b*) M. Irie, Special Issue: Photochromism: Memories and Switches, *Chem. Rev.*, 2000, **100**, 1683–1890; (*c*) G. Mayer and A. Heckel, *Angew. Chem., Int. Ed.*, 2006, **45**, 4900–4921; (*d*) M.-M. Russew and S. Hecht, *Adv. Mater.*, 2010, **22**, 3348–3360.

8 D. Bléger, Z. Yu and S. Hecht, *Chem. Commun.*, 2011, **47**, 12260–12266.

9 (*a*) M. V. Peters, R. S. Stoll, A. Kühn and S. Hecht, *Angew. Chem., Int. Ed.*, 2008, **47**, 5968–5972; (*b*) R. S. Stoll, M. V. Peters, A. Kühn, S. Heiles, R. Goddard, M. Bühl, C. M. Thiele and S. Hecht, *J. Am. Chem. Soc.*, 2009, **131**, 357–367.

10 (*a*) C. Tie, J. C. Gallucci and J. R. Parquette, *J. Am. Chem. Soc.*, 2006, **128**, 1162–1171; (*b*) E. D. King, P. Tao, T. T. Sanan, C. M. Hadad and J. R. Parquette, *Org. Lett.*, 2008, **10**, 1671–1674; (*c*) Y. Hua and A. H. Flood, *J. Am. Chem. Soc.*, 2010, **132**, 12838–12840; (*d*) Y. Wang, F. Bie and H. Jiang, *Org. Lett.*, 2010, **12**, 3630–3633; (*e*) H. Sogawa, M. Shiotsuki, H. Matsuoka and F. Sanda, *Macromolecules*, 2011, **44**, 3338–3345.

11 (*a*) A. Khan, C. Kaiser and S. Hecht, *Angew. Chem., Int. Ed.*, 2006, **45**, 1878–1881; (*b*) A. Khan and S. Hecht, *Chem.–Eur. J.*, 2006, **12**, 4764–4774; (*c*) Z. Yu and S. Hecht, *Angew. Chem., Int. Ed.*, 2011, **50**, 1640–1643.

12 Z. Yu and S. Hecht, *Chem.–Eur. J.*, 2012, **18**, 10519–10524.

13 M. T. Stone, J. M. Heemstra and J. S. Moore, *Acc. Chem. Res.*, 2006, **39**, 11–20.

14 (*a*) J. E. Lovett, M. Hoffmann, A. Cnossen, A. T. J. Shutter, H. J. Hogben, J. E. Warren, S. I. Pascu, C. W. M. Kay, C. R. Timmel and H. L. Anderson, *J. Am. Chem. Soc.*, 2009, **131**, 13852–13859; (*b*) J. Wang, L. Hou, W. R. Browne and B. L. Feringa, *J. Am. Chem. Soc.*, 2011, **133**, 8162–8164.

15 C. R. Ray and J. S. Moore, *Adv. Polym. Sci.*, 2005, **177**, 99–149.

16 For general introduction of occurrence of Cotton effect in CD spectra, see: (*a*) N. Berova, K. Nakanishi and R. W. Woody, *Circular Dichroism: Principles and Applications*, Wiley, New York, 2nd edn, 2000; (*b*) D. A. Lightner and J. E. Gurst, *Organic Conformational Analysis and Stereochemistry from Circular Dichroism Spectroscopy*, Wiley, New York, 2000, p. 423 and references therein.

17 R. B. Prince, J. G. Saven, P. G. Wolynes and J. S. Moore, *J. Am. Chem. Soc.*, 1999, **121**, 3114–3121.

18 (*a*) R. B. Prince, L. Brunsveld, E. W. Meijer and J. S. Moore, *Angew. Chem., Int. Ed.*, 2000, **39**, 228–230; (*b*) R. B. Prince, J. S. Moore, L. Brunsveld and E. W. Meijer, *Chem.–Eur. J.*, 2001, **7**, 4150–4154.

19 The concentration-dependent aggregation of related foldamers has been investigated thoroughly, see: M. T. Stone, J. M. Heemstra and J. S. Moore, *Acc. Chem. Res.*, 2006, **39**, 11–20. The concentration used in our experiments is beyond the critical aggregation concentration.

20 For reviews on π,π-stacking interactions, consult: (*a*) C. A. Hunter, K. R. Lawson, J. Perkins and C. J. Urch, *J. Chem. Soc., Perkin Trans. 2*, 2001, 651–669; (*b*) E. A. Meyer, R. K. Castellano and F. Diederich, *Angew. Chem., Int. Ed.*, 2003, **42**, 1210–1250.

21 For the details of determining the incomplete folding behavior of oligomer $\mathbf{10_5}$, that is in equilibrium with its unfolded state, see ref. 11*c*

22 B. H. Zimm and J. K. Bragg, *J. Chem. Phys.*, 1959, **31**, 526–535.

23 Note that in the other two foldamer series these thermodynamic parameters cannot be derived, either because of missing data points (in the case of the 1.5 azos/

turn series) or due to absence of Ph–Ph contacts at the termini (in the case of the 2 azos/turn series). For the calculation of ΔG_{nuc} and ΔG_{prop} for 3 azos/turn foldamer series, see the ESI, S6.‡

24 Here, the *Z*-isomers refer to the oligomeric isomers in any conformation containing at least one *Z*-azobenzene unit.

25 (*a*) H. Rau and E. Lüddecke, *J. Am. Chem. Soc.*, 1982, **104**, 1616–1620; (*b*) T. Nägele, R. Hoche, W. Zinth and J. Wachtveitl, *Chem. Phys. Lett.*, 1997, **272**, 489–495; (*c*) Y.-C. Lu, E. W.-G. Diau and H. Rau, *J. Phys. Chem. A*, 2005, **109**, 2090–2099.

26 Note that the thermal induced relaxation of the sample from the PSS back to the thermodynamic equilibrium is extremely slow in acetonitrile. To allow for the measurements over a more reasonable time frame, aqueous acetonitrile solution (20% H_2O in CH_3CN) was used throughout the experiments to further stabilize the folded products and hence accelerate the renaturation process. Although clear isodichroic points were found in all CD spectra, the partial formation of foldamer aggregates cannot be ruled out, because of the observation of a temperature-dependence of the maximum molar circular dichroism of the completed refolding oligomer in the CD spectra, see: L. Brunsveld, E. W. Meijer, R. B. Prince and J. S. Moore, *J. Am. Chem. Soc.*, 2001, **123**, 7978–7984. Nevertheless, the results of the investigated oligomers were obtained under the same conditions allowing for a true comparison of the refolding behavior.

27 Note a slight deviation from first-order refolding in the case of $\mathbf{14}_7$ presumably due to the high degree of cooperativity leading to more sigmoidal behavior.

28 H. Eyring, *Chem. Rev.*, 1935, **17**, 65–77.

29 (*a*) J. C. van Miltenburg and J. A. Bouwstra, *J. Chem. Thermodyn.*, 1984, **16**, 61–65; (*b*) J. C. van Miltenburg and J. A. Bouwstra, *J. Chem. Thermodyn.*, 1985, **17**, 685–695.

30 (*a*) T. Asano, T. Okada, S. Shinkai, K. Shigematsu, Y. Kusano and O. Manabe, *J. Am. Chem. Soc.*, 1981, **103**, 5161–5165; (*b*) W.-H. Wei, T. Tomohiro, M. Kodaka and H. Okuno, *J. Org. Chem.*, 2000, **65**, 8979–8987; (*c*) Y. Norikane, K. Kitamoto and N. Tamaoki, *J. Org. Chem.*, 2003, **68**, 8291–8304.

31 In the corresponding experiments, the PSS of the investigated samples was reached in chloroform and subsequently transferred to acetonitrile for CD measurements.

32 The shape of the curves in Fig. 6 (center) is indeed indicative of a cooperative thermal refolding process, in particular since an alternative isodesmic process can be excluded. For more details, see: M. M. J. Smulders, M. M. L. Nieuwenhuizen, T. F. A. de Greef, P. van der Schoot, A. P. H. J. Schenning and E. W. Meijer, *Chem.–Eur. J.*, 2010, **16**, 362–367.

33 (*a*) V. Daggett, *Chem. Rev.*, 2006, **106**, 1898–1916; (*b*) E. Shakhnovich, *Chem. Rev.*, 2006, **106**, 1559–1588; (*c*) E. Chen, J. R. Kumita, G. A. Woolley and D. S. Kliger, *J. Am. Chem. Soc.*, 2003, **125**, 12443–12449; (*d*) B. Adisa and D. A. Bruce, *J. Phys. Chem. B*, 2005, **109**, 7548–7556; (*e*) P. Tao, J. R. Parquette and C. M. Hadad, *J. Chem. Theory Comput.*, 2012, **8**, 5137–5149.

34 For a representative example using X-ray scattering to monitor the geometrical size of foldamer in solution with extremely high concentration, see: R. F. Kelley, B. Rybtchinski, M. T. Stone, J. S. Moore and M. R. Wasielewski, *J. Am. Chem. Soc.*, 2007, **129**, 4114–4115.

35 (*a*) A. Godt, M. Schulte, H. Zimmermann and G. Jeschke, *Angew. Chem., Int. Ed.*, 2006, **45**, 7560–7564; (*b*) G. Jeschke, M. Sajid, M. Schulte, N. Ramezanian, A. Volkov, H. Zimmermann and A. Godt, *J. Am. Chem. Soc.*, 2010, **132**, 10107–10117.

36 For a leading example of qualitative ESR evaluation of solvent-induced conformational transition, see: K. Matsuda, M. T. Stone and J. S. Moore, *J. Am. Chem. Soc.*, 2002, **124**, 11836–11837.

37 The spectra of foldamer $\mathbf{11}_4$**-TEMPO** was used as a reference spectrum, which shown no sign of intermolecular spin-coupling interaction.

38 For details, see ESI.‡

39 Please note that the smallest distances found here are needed to describe the outer wings of the spectrum correctly. In particular the spectral contribution arising from a distance of 0.9 nm is found at the onset of the spectrum and thus particularly susceptible to experimental details such as baseline stability.

40 A. I. Korkorin, K. I. Zamarayev, G. L. Grigoryan, V. P. Ivanov and E. G. Rozantsev, *Biofizika*, 1972, **17**, 34–41.

41 K. C. Neuman and A. Nagy, *Nat. Methods*, 2008, **5**, 491–505.

42 M. von Delius and D. A. Leigh, *Chem. Soc. Rev.*, 2011, **40**, 3656–3676.

43 (*a*) T. Hugel, N. B. Holland, A. Cattani, L. Moroder, M. Seitz and H. E. Gaub, *Science*, 2002, **296**, 1103–1106; (*b*) V. Ferri, M. Elbing, G. Pace, M. Dickey, M. Zharnikov, P. Samorì, M. Mayor and M. Rampi, *Angew. Chem., Int. Ed.*, 2008, **47**, 3407–3409; (*c*) M. Yamada, M. Kondo, J.-I. Mamiya, Y. Yu, M. Kinoshita, C. Barrett and T. Ikeda, *Angew. Chem., Int. Ed.*, 2008, **47**, 4986–4988.